INTERNATIONAL JOURNAL FOR NUMERICAL METHODS IN FLUIDS, VOL. 23, 1085–1109 (1996)

ON THE STRUCTURE OF STEADY FLOW THROUGH DUAL-INTAKE ENGINE PORTS

Z. MAHMOOD, A. CHEN AND M. YIANNESKIS

Centre for Heat Transfer and Fluid Flow Measurement, Mechanical Engineering Department, King's College London, Strand, London WC2R 2LS, U.K.

AND

G. GANTI

Research and Engineering Centre, Ford Motor Company Limited, Laindon, Essex SS15 6EE, U.K.

SUMMARY

The influence of intake port design on the flow field in a dual-intake valve engine was investigated using computational fluid dynamics, in order to study the effect of inlet port design on the in-cylinder flow. A detailed 3D computational grid incorporating all the features of the Ford Zetec production engine inlet ports, valves and cylinder head was initially created and the flow structure modelled at 5 and 10 mm valve lifts under steady flow conditions. Comparisons of computational results with experimental data obtained by laser Doppler anemometry indicate that the flow characteristics have been predicted well in most regions. Flow generated by different intake port designs was also simulated by introducing air into the cylinder at different directions to the inlet valve axes and the effects of port deactivation, throttling and exhaust gas recirculation were examined. The implications of the results for intake port design are discussed.

KEY WORDS: intake port; dual intake; CFD; laser Doppler anemometry; internal combustion engine; cylinder; turbulence; steady flow

1. INTRODUCTION

Increasing public concern regarding environmental issues in the last two decades has resulted in the introduction of stringent world-wide pollutant emission regulations. Many of the requirements set by governmental organizations in recent years with regard to emissions and fuel economy have been met through the introduction of multivalve engines in modern cars. In addition, increasing the number of intake valves in a spark ignition (SI) engine allows the engine torque and speed to be increased and can help achieve higher specific power output.

In dual-intake valve SI engines, tumble motion has been noted to offer good possibilities for the optimization of turbulence and combustion parameters. During the compression stroke the tumble vortex experiences 'spin-up', where its rotational velocity about its axis increases as it is compressed.[1] High levels of turbulence are generated owing to breakdown of tumble close to TDC of compression, prior to ignition of the air–fuel mixture.

CCC 0271–2091/96/101085–25

Received September 1995
Revised February 1996

The flow fields inside multivalve engines have been investigated using both experimental and computational techniques. Khalighi[2] studied the development of swirl and tumble in five different intake valve configurations. It was found that when both inlet valves are open, no well-defined tumble flow structure is created and vortices dissipate quickly before the piston reaches BDC of the induction stroke. However, the strongest tumble flow at BDC of induction was generated when one intake valve was kept closed and a 180° shroud was attached to the open valve. The effect of tumble intensity during induction on pre-combustion turbulence was investigated by Rönnbäck *et al.*[3] in low-, medium- and high-tumble intake systems using particle-tracking velocimetry. The medium- and high-tumble cylinder heads produced higher values of tumble ratio and it was shown that a high-intensity tumble vortex will produce larger turbulent length scales and higher turbulence intensities in the flow field prior to combustion.

Furuno *et al.*[4] investigated how the inclination of swirling flows affects turbulence characteristics. A swirl control valve fitted to one port and a port with a variable angle shroud were used to vary flow inclination. Furuno *et al.* observed that the turbulence intensity generated between 30° BTDC and TDC of the compression stroke varies greatly with the inclination angle of the swirling flow. The highest turbulence intensity near TDC of compression occurs when the swirl is inclined between 30° and 45°. Arcoumanis *et al.*[5] performed tests on a low- and a high-tumble cylinder head to assess the suitability of four-valve cylinder heads to produce tumble under steady flow conditions. The tumble intensity rose as intake valve lifts were increased above 3 mm. Measurements in a motored optical engine indicated that the tumble ratio reaches a maximum at 280° CA and 320°CA, corresponding to the 'spin-up' process described earlier.

Four-valve engines employing high-tumble induction systems have been noted to result in lower combustion times in addition to reductions in harmful exhaust emissions. De Boer *et al.*[6] assessed the combustion characteristics of three engines fitted with low- to high-tumble cylinder heads. High-tumble systems gave rise to the lowest ignition delays and combustion durations throughout the air–fuel ratio (AFR) range tested. Moreover, de Boer *et al.* note that the higher exhaust gas recirculation (EGR) tolerance of a high-tumble system resulted in reductions in pumping losses, leading directly to a gain of 3 per cent–6 per cent in fuel economy. Hydrocarbon and CO emissions from the engine were reduced by 18 per cent and 25 per cent respectively. Similar trends were also observed by Endres *et al.*,[7] who compared engines offering different levels of tumble and swirl intensity with a four-valve engine having conventional ports. The high-tumble system had the lowest ignition delay, almost half that produced by the conventional port design. The same trend was observed for the combustion duration. Endres *et al.* also found that the greater tolerance to EGR allowed by swirl and tumble systems resulted in a reduction of approximately 4 per cent in the specific fuel consumption compared with the conventional system. By combining swirl and/or tumble with EGR, a reduction in NO_x emissions of up to 80 per cent was reported.

Stratification of the charge in a multivalve engine, either radially or laterally, leads directly to improved combustion and emissions characteristics, as typified by the Mitsubishi Vertical Vortex engine,[8] the Ricardo Combustion Control by Vortex Stratification system[9] and Hyundai's axially stratified lean combustion engine.[10] By making use of a strong tumble of swirl flow to stratify stoichiometric fuel mixture and EGR, substantial reductions in vehicle fuel consumption, cyclic variation in combustion and exhaust emissions are acquired in comparison with similar homogeneous charge engines.

This paper describes an investigation of the flow through the Ford Zetec engine ports using both computational fluid dynamics (CFD) and laser Doppler anemometry (LDA). The engine was developed with a view to maintaining the high specific power output characteristics of multivalve engines without compromising on combustion quality. The fixed geometry, siamese intake port design of the cylinder head offers good volumetric efficiency and encourages the generation of

tumble in the engine.[11] In order to model accurately the shape of the engine, a detailed three-dimensional numerical grid of the engine inlet ports and cylinder was produced using CFD. Flow motion was modelled under steady flow conditions and compared with the experimental data to assess the accuracy of the predictions. Subsequently CFD investigations of the influence of intake jet direction on in-cylinder flow were made without modelling the intake ports, in order to simulate different designs of intake port, and the effects of port deactivation, throttling and EGR were also studied.

2. FLOW CONFIGURATION AND EXPERIMENTAL TECHNIQUES

The intake port and cylinder head geometry are shown in Figure 1. The present work was performed on the 1·8 l engine model, so that the cylinder bore is 80·6 mm and the inlet valve head diameter is 32 mm. The ensemble-averaged mean velocity components, U, V, W and the corresponding RMS components u', v', w' were defined in the co-ordinate directions x, y and z respectively shown in Figure 1.

The experiments were performed under steady flow conditions using a Perspex replica of the intake ports and cylinder of the Zetec engine. A mixture of oil or turpentine and tetraline liquids in the proportions 68 : 32 by volume was employed as the working fluid. The experimental rig comprised a closed-circuit liquid tunnel; there was no piston in the cylinder, so that the liquid flowed out of the cylinder and was recirculated via a pump, a variable-area flowmeter and a constant-head tank to the inlet of the Perspex replica. When the mixture temperature was maintained at 25°C, its refractive index (1·489) and that of the Perspex material were identical, allowing optical access to laser beams for LDA measurements. Laser sheet flow visualization recordings were also made to identify the main flow features. The density of the mixture was 893·5 kg m^{-3} and its kinematic viscosity was $1{\cdot}71 \times 10^{-6}$ m^2 s^{-1}. Measurements were obtained at a Reynolds number (Re) of 30,000 ($Q_T = 1{\cdot}54$ kg s^{-1}) with both lifts at 5 mm and then at 10 mm and also at Re = 19,500, 24,500

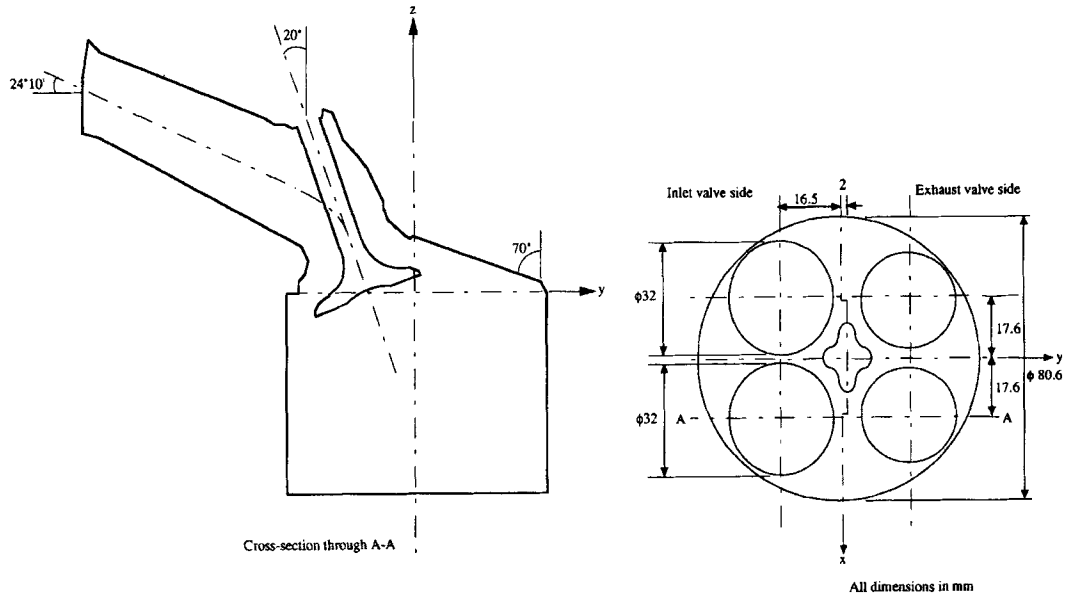

Figure 1. Outline of Ford Zetec engine intake port in a vertical plane thorugh one inlet valve and cylinder head dimensions

and 30,000 with one valve closed and the other at 10 mm lift to determine flow rate effects. Turbulent flow was achieved in the intake ports and cylinder for all *Res* studied. The similarity of liquid and air flows through engine inlet ports has been previously established.[12]

The laser Doppler anemometer was operated in the forward-scatter fringe mode. The anemometer comprised a 10 mW helium–neon laser, a rotating diffraction grating to split the laser beam and to provide a frequency shift between the two first-order beams, a photomultiplier and associated optics. For signal processing, a frequency counter and a computer interfaced to the counter and installed with data-processing software were employed. Artificial seeding of the flow as not necessary, as the liquid mixture contained a sufficient number of micron-sized contaminant particles. Further details of the experimental techniques are provided in Reference 13.

3. COMPUTATIONAL MODEL

The flows were simulated using the STAR-CD CFD programme.[14] Turbulence was modelled with the k–ε model and a 'law of the wall' formulation was specified at all solid surfaces. The SIMPISO solution algorithm[14] was employed with an upwind differencing scheme. Although this scheme may result in considerable numerical diffusion, its suitability has been established through extensive tests carried out in earlier work on steady flows through engine ports.[15] The SIMPISO algorithm is similar to the well-known SIMPLE method but is designed to perform better with severely distorted meshes. The algorithm performs one momentum corrector but incorporates the more elaborate treatment of the additional pressure terms arising from grid non-orthogonality which is employed in the PISO algorithm.[16] The computational time requirement per iteration of SIMPISO is therefore greater than that of SIMPLE and an additional relaxation factor must be specified for the pressure calculation. Figure 2(a) presents the three-dimensional grid for the inlet ports and cylinder of the Ford Zetec engine, while Figure 2(b) provides a cross-sectional view of the grid in a vertical plane through the centre of one inlet valve.

Three sets of CFD predictions were performed. First, flow of the liquid mixture through the complete inlet ports and cylinder of the Zetec engine was modelled with both valve lifts set first at 5 mm and then at 10 mm, so that the flow predictions could be assessed against the LDA data. The flow rate was prescribed as $Q_T = 1{\cdot}54$ kg s^{-1} and the fluid properties were identical with those of the liquid mixture used in the experiments. Second, the similarity of air and liquid flows was established through calculations with the two fluids at *Res* of 19,500, 24,500 and 30,000. The air temperature and density were specified as 20°C and 1·20 kg m^{-3} respectively.

Third, the effect of different types of inlet port on in-cylinder flow was examined by varying the direction of the intake flow into the cylinder, although the ports themselves were not modelled. Port throttling, deactivation and EGR were also simulated. The inlet valve lift was set at 10 mm for all cases. The fluid medium was air and inlet boundary conditions were specified in the annular region between the port and the valve stem immediately upstream of the valve seat, based on the air mass flow rate. $Q_{P1} = 0{\cdot}03216$ kg s^{-1} in all cases, while Q_{P2}-values of 0, 0·01286 and 0·03216 kg s^{-1} were used to simulate port deactivation, throttling and wide-open throttle operation respectively. Flow visualization and LDA results have shown that a recirculation region is formed at the exit of the port by the flow passing over the back of the inlet valve and into the cylinder. This separation region was modelled in some of the CFD calculations as a solid wall.

The numerical grid including the inlet ports contained 68,822 cells for both the 5 and 10 mm valve lift cases. The grid size and structure were based on earlier experience with similar port flows,[15] in which it was established that grid-independent solutions could be obtained with grids of this size. This was confirmed by the grid sensitivity test described below. A cylinder length of 134·3 mm was modelled. This length was selected to be sufficient to accommodate the vortex formed below the

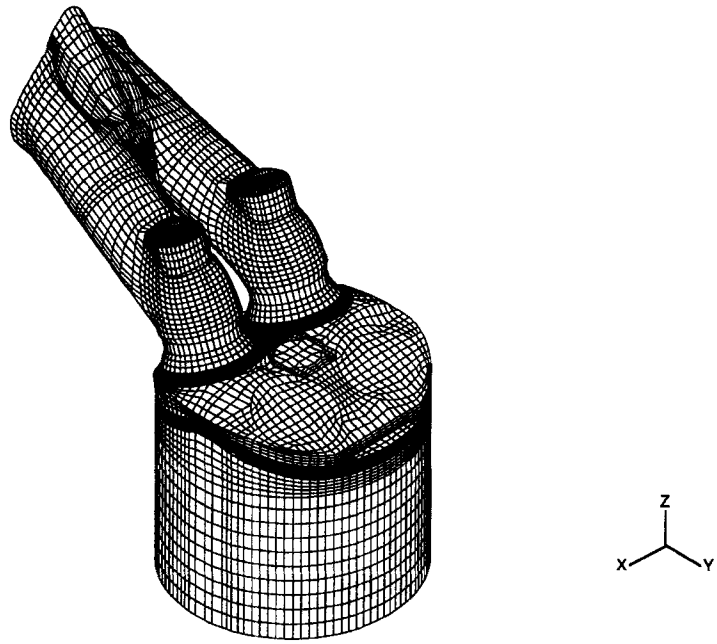

Figure 2(a). Three-dimensional grid for inlet ports and cylinder of engine

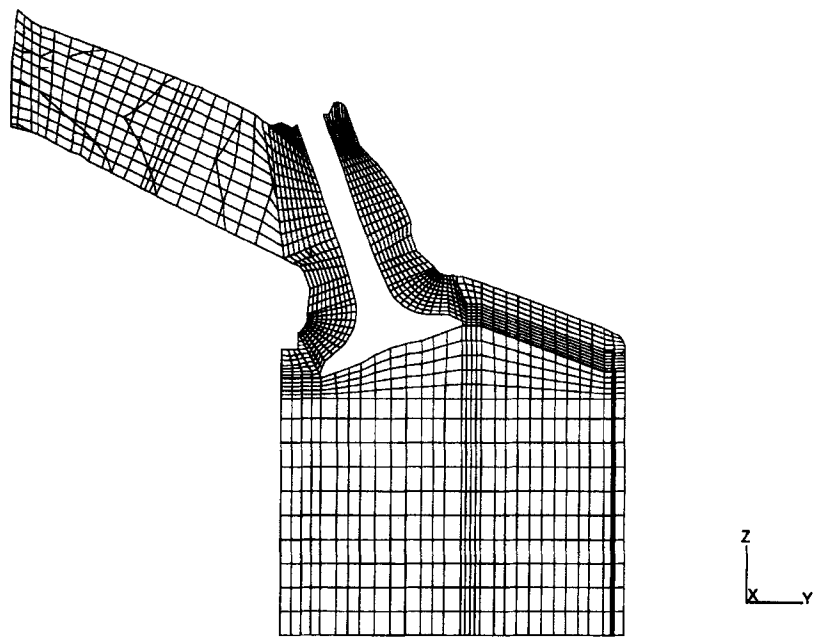

Figure 2(b). Cell structure within vertical plane $x = -17{\cdot}6$ mm at a valve lift of 10 mm

valve and have no effect on the outlet conditions of the calculation domain. The inlet boundary condition was defined at the entry plane of the inlet ports and the outlet boundary condition was specified at the cylinder exit plane. The velocity distribution at the inlet plane was designated as a uniform mean velocity profile based on the measured or specified flow rate. The outlet boundary conditions specified at the cylinder exit plane were that the flow at all locations in this plane would be directed outwards and that continuity was satisfied at the exit.

The generation of the surface grid for the ports and cylinder was based on CAD data provided by Ford. The internal grid structure was selected on the basis of experience gained from earlier CFD studies of generic ports, so that highly concentrated grid lines were located in regions of steep velocity gradients. The co-ordinate position of the vertices in the vicinity of the walls was input manually to match the surface specified by the CAD data with the internal grid structure. In order to determine the grid independence of the solutions obtained, grid sensitivity tests were carried out. The total number of cells across the flow field was increased by 26 per cent, with the additional cells either concentrated in regions around the valve stem or distributed across the entire field. The variations in the mean flow and turbulence results with grid size in both cases were smaller than the specified convergence criteria and it was established that the solutions were independent of grid size.

4. RESULTS AND DISCUSSION

4.1. Flow structure with production intake ports

Predicted flow field at 5 and 10 mm valve lifts. The computed velocity vectors in the vertical plane through the centre of one valve, $x = -17{\cdot}6$ mm, for a lift of 5 mm and liquid flow with $Q_T = 1{\cdot}54$ kg s^{-1} are shown in Figure 3(a). Velocities inside the port increase on approach to the stem. A high-velocity jet flows over the valve. A small tumble-like vortical flow motion is created by the intake jet to the right of the valve in Figure 3(a). An elliptically shaped vortex is produced by fluid passing on the left of the valve. The two vortices form part of a toroidal ring vortex inside the cylinder. A flow akin to a wall jet can be seen against the cylinder wall, while velocity magnitudes near the centre of the cylinder are low, especially underneath the valve.

In horizontal x–y planes a symmetric flow structure is created about the plane of symmetry of the cylinder head, $x = 0$ mm, even though no conditions of symmetry were applied to the flow. This is evident in Figure 3(b), which shows velocity vectors in the $z = -10$ mm plane. The flow field comprises primarily two counter-rotating vortices, one on either side of the $x = 0$ mm plane, with two weaker vortices also evident near the centre of the plane and a jet motion in the centre of the cylinder as the fluid travels away from the inlet valves and towards the right. The region beneath the inlet valves is shown on the left of Figure 3(b); the low horizontal velocity magnitudes there indicate that the flow is moving mainly downwards.

When the inlet valve lift is increased from 5 to 10 mm while maintaining the mass flow rate of 1·54 kg s^{-1}, differences in the flow are observed. Figure 4(a) displays the flow field in the $x = -17{\cdot}6$ mm plane. Velocity magnitudes inside the port are very similar to those computed with the 5 mm lift. Importantly, a separation region is formed around the valve seat, to the left of the valve. The higher lift results in an intake jet of greater cross-section to the right of the valve than in Figure 3(a) and consequently velocities inside the jet are lower. The highest velocity predicted in this plane, 2·75 m s^{-1}, is in the valve gap. Qualitatively the flow patterns below the valve are similar to those at 5 mm lift, but there are differences, e.g. in the size of the vortices.

Velocity vectors in the $z = -10$ mm plane for the 10 mm lift are presented in Figure 4(b). As was noted in Figure 3(b), the flow structure consists of two pairs of counter-rotating vortices in the region underneath the inlet valves, although these are smaller in size than those observed with the 5 mm lift.

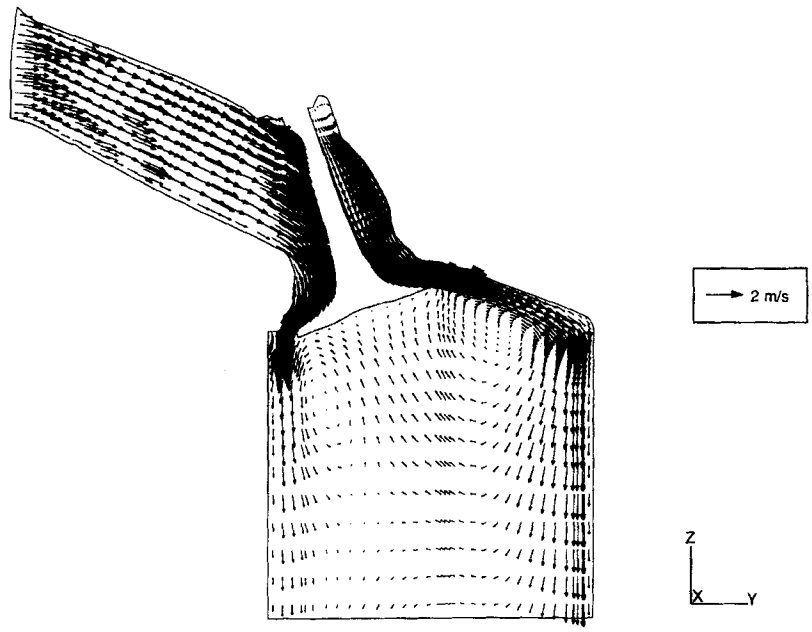

Figure 3(a). Computed velocity vectors in vertical plane $x = -17{\cdot}6$ mm at a valve lift of 5 mm

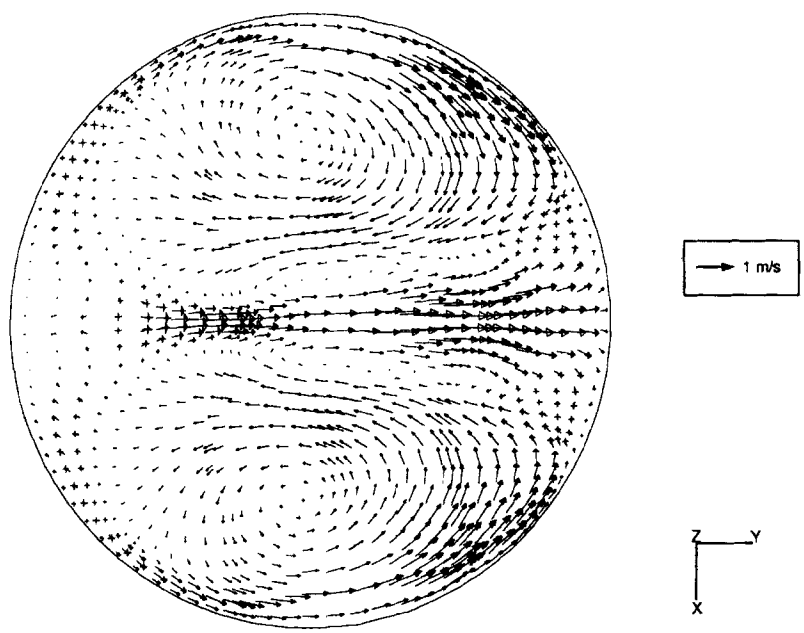

Figure 3(b). Computed velocity vectors in horizontal plane $z = -10$ mm at a valve lift of 5 mm

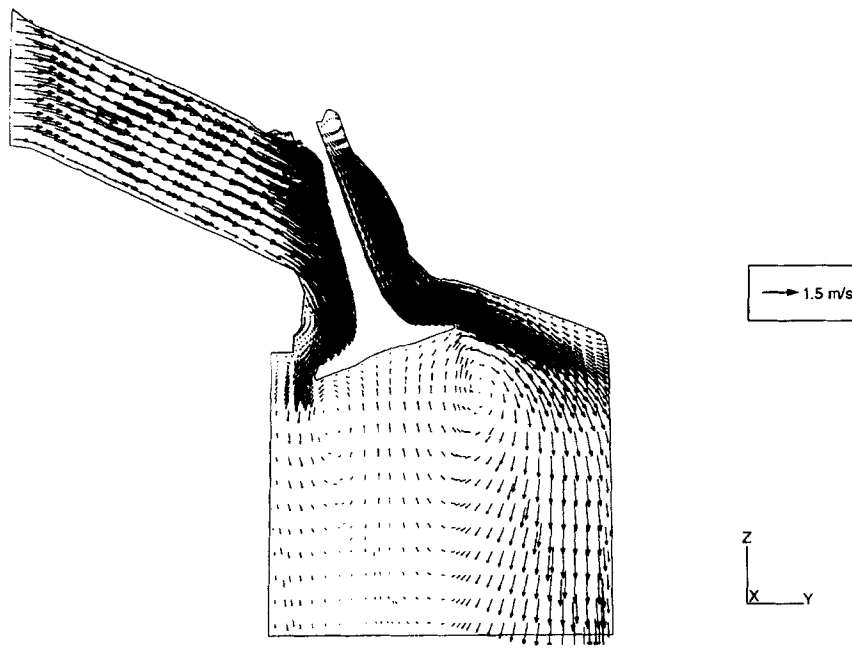

Figure 4(a). Computed velocity vectors in vertical plane $x = -17{\cdot}6$ mm at a valve lift of 10 mm

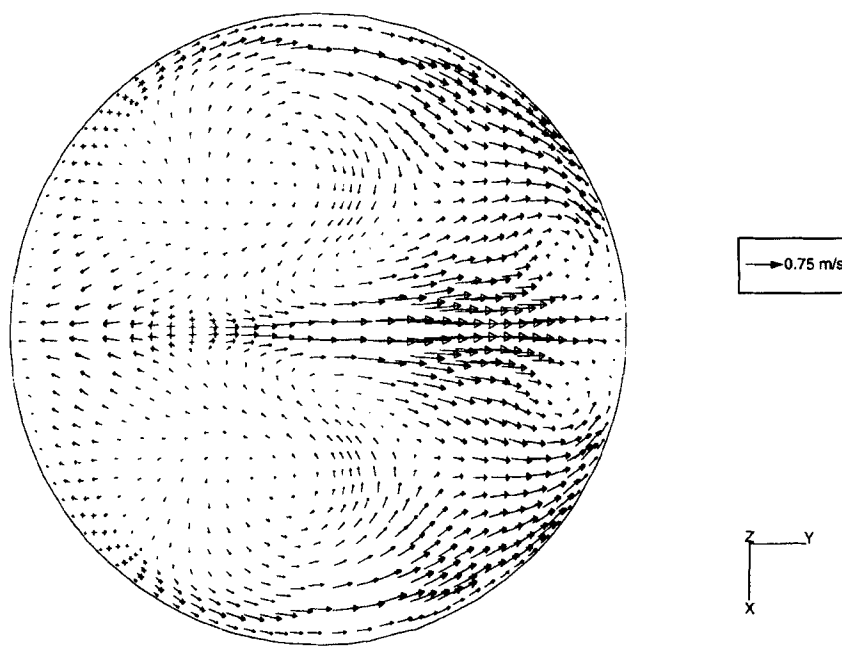

Figure 4(b). Computed velocity vectors in horizontal plane $z = -10$ mm at a valve lift of 10 mm

The combination of the flows over the two valves again produces a jet travelling across the cylinder away from the valves, which is formed from the cylinder centre to the right wall. Regions of low velocity magnitude are identifiable at the left- and right-hand edges of Figure 4(b), in which the flow has a primarily vertical velocity component.

The predictions of the kinetic energy of turbulence (k), not shown for economy of presentation, indicated that when the valve lift is set at 5 mm, turbulence levels are low inside the majority of the inlet port region, 0·0063 $m^2\ s^{-2}$ at the port entry and along the port walls and 0·0569 $m^2\ s^{-2}$ close to the stem. The highest levels of k, 0·1708 $m^2\ s^{-2}$, are encountered at the valve lip, on either side of the valve. The majority of the in-cylinder region has low levels of k, particularly near the cylinder walls. Turbulence levels are, on the whole, lower for the 10 mm than for the 5 mm valve lift, but k-values inside the port are similar for both lifts. The highest value of k is again encountered at the valve lip, 0·125 $m^2\ s^{-2}$. The intake jets for the 10 mm lift have valves of k around 60 per cent lower owing to the smaller velocity gradients encountered in the valve gap. In the main, k-levels are low over most of the cylinder as for the 5 mm lift.

Comparison of predictions and measurements. Figure 5(a) presents a comparison of the measured and computed vertical (W- component) velocities in the $x = -17{\cdot}6$ mm plane at a valve lift of 5 mm. The figure shows very good agreement between the CFD and LDA results in most regions. The flow motion to the right of the valve in Figure 5(a) has been very well predicted and the computed and measured W-velocity magnitudes are very similar. Close to the left wall of the cylinder there is qualitative agreement between the LDA and CFD results, but the measurements show steeper velocity gradients than the predictions. The LDA and CFD results in the $z = -30$ mm horizontal plane, presented in Figure 5(b), show excellent qualitative and good quantitative agreement in most regions.

Close matching of numerical and experimental W-velocity results is also achieved for the 10 mm lift in the $x = -17{\cdot}6$ mm plane, as Figure 5(c) illustrates. Both sets of results identify the tumbling structure to the right of Figure 5(c), in addition to the anticlockwise-rotating vortex created by flow to

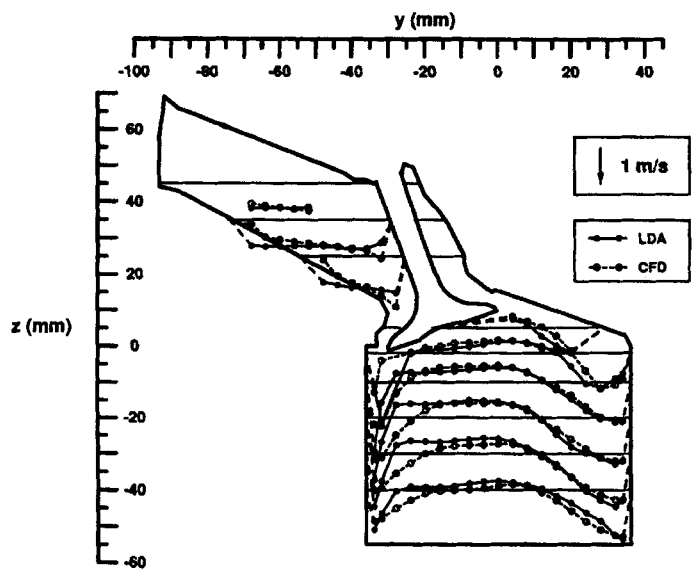

Figure 5(a). Comparison of measured and calculated W-component velocities in vertical plane $x = -17{\cdot}6$ mm at a valve lift of 5 mm

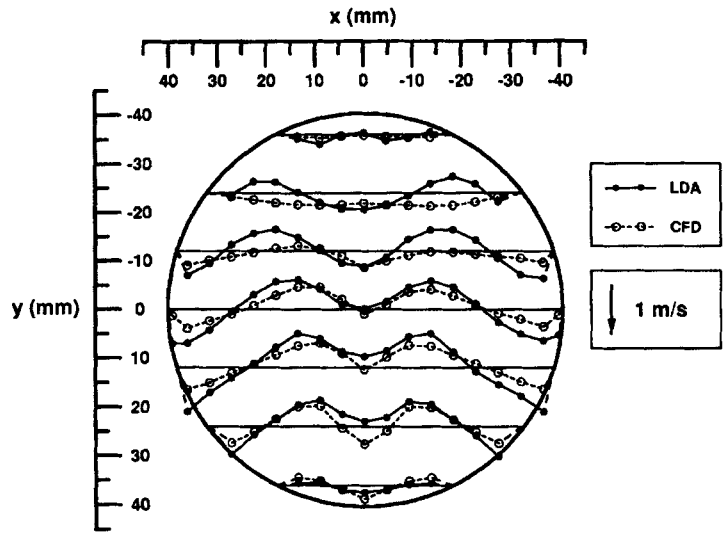

Figure 5(b). Comparison of measured and calculated V-component velocities in horizontal plane $z = -30$ mm at a valve lift of 5 mm

the left of the valve. However, some differences can be noted at locations close to the right cylinder wall.

LDA and CFD results in the $z = -30$ mm plane are compared in Figure 5(d). The computed and measured V-velocity results show similarities at most locations. The experimental results indicated a small asymmetry in the flow towards the front of the cylinder, shown in the $y = 24$ and 36 mm velocity profiles in Figure 5(d). This asymmetry is believed to be caused by uneven splitting of the

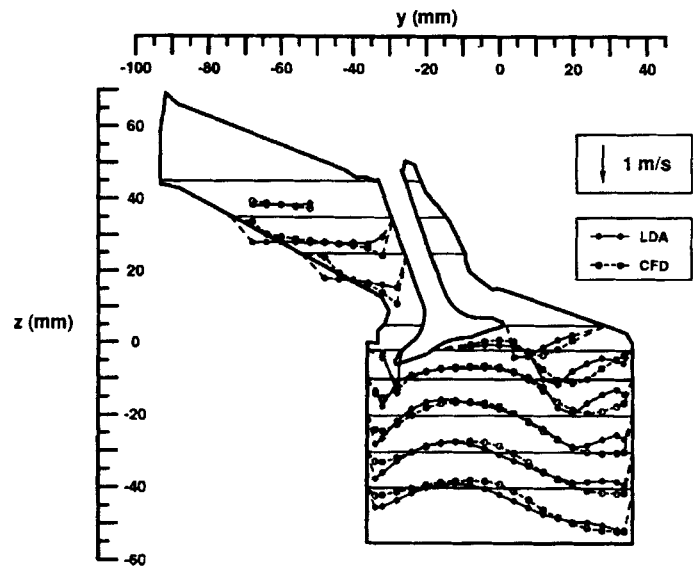

Figure 5(c). Comparison of measured and calculated W-component velocities in vertical plane $x = -17{\cdot}6$ mm at a valve lift of 10 mm

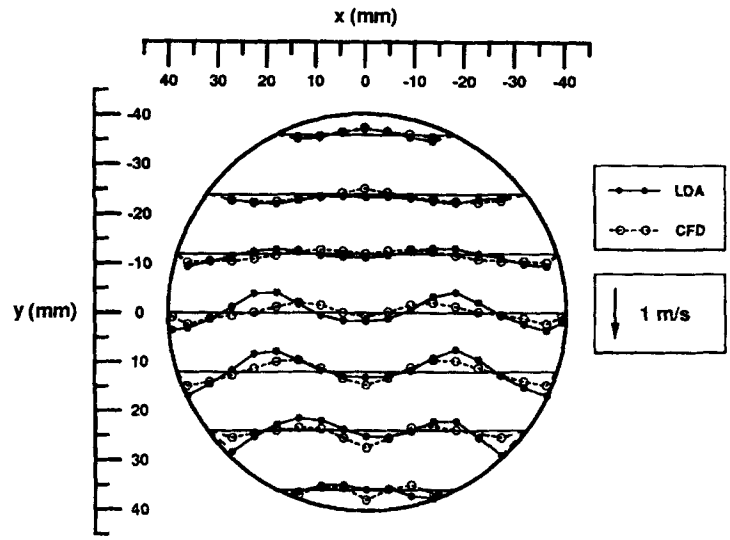

Figure 5(d). Comparison of measured and calculated V-component velocities in horizontal plane $z = -30$ mm at a valve lift of 10 mm

flow at the entrance to the ports, despite the lifts for both valves being identical. This was verified by a CFD prediction with 45 per cent of the mass flow rate through one port and 55 per cent through the other, which revealed a flow asymmetry similar to but more pronounced than, that described above. The inlet ports of the experimental test section were geometrically symmetrical about the $x = 0$ mm plane, so that the uneven split of the flow could not have been caused by asymmetries in the test section and further investigation is necessary to identify the origin of this slight flow asymmetry.

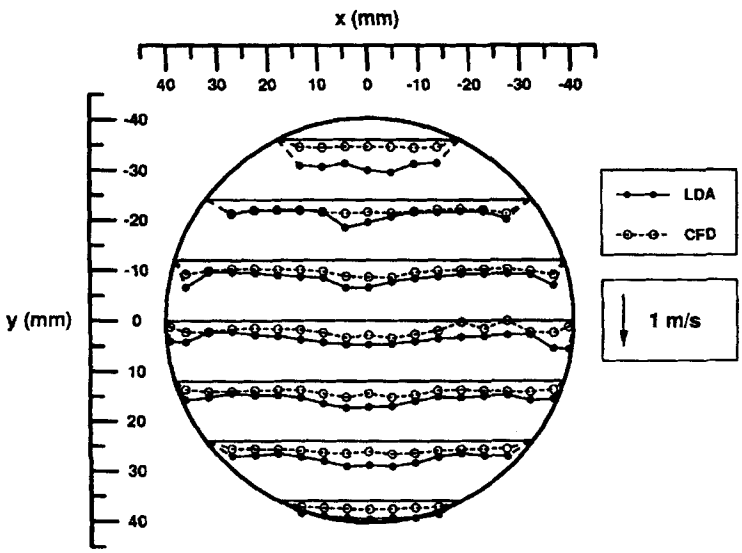

Figure 5(e). Comparison of measured and calculated RMS v'-component velocities in horizontal plane $z = -10$ mm at a valve lift of 5 mm

Predictions of k for both valve lifts have been examined by comparing the measured RMS velocities with those evaluated from the predictions using the expression $u' = v' = w' = (2k/3)^{0.5}$. Figure 5(e) presents profiles of v' in the $z = -10$ mm plane for the 5 mm lift. It is apparent that v'-magnitudes are underpredicted on the whole and more so in regions of high shear, such as near the cylinder wall and centre. The implicit assumption of isotropic turbulence in the formulation of the k–ε turbulence model may partly account for the underprediction of the RMS quantities, as the experimental results have indicated that this assumption is not applicable for many regions of the flow. Moreover, previous investigations have revealed the presence of instabilities in the flow, such as 'flapping' of the intake jet as the fluid passes over the valve,[15] which are not modelled by the CFD programme. Time-resolved velocity measurements can provide a better indication of the mean and RMS velocity variations if the non-random fluctuation components are removed from the velocity results using fast Fourier transform (FFT) and inverse FFT techniques. Such techniques have been successfully applied to remove the broadening of the RMS values caused by mean flow variation due to vortex shedding in the flows past rod bundles and have yielded considerably lower RMS values, in agreement with related CFD predictions.[17]

Effect of mass flow rate and working fluid. In order to ensure that in- cylinder flow velocities scaled with mass flow rate under steady flow conditions, CFD and LDA flow rate tests were carried out. Three Q_T-values were selected for liquid flow for each of the valve lifts studied: 0·98 kg s^{-1} (Re = 19,000), 1·26 kg s^{-1} (Re = 24,500) and 1·54 kg s^{-1} (Re = 30,000). The CFD results showed no change in flow structure at each of the three flow rates, and mean velocities scaled with liquid mass flow rate. Identical flow structures were produced when air and liquid flows were modelled with the same Re. For the LDA flow rate tests, in view of the slight asymmetry in one part of the flow noted at 10 mm lift earlier, mean and RMS velocity measurements were made with one intake valve completely closed and the other having a 10 mm valve lift, so that all the liquid mixture flowed through only one of the inlet ports and uneven split of the flow, however minor, was not possible. When Q_{P1} was varied from 0·98 to 1·54 kg s^{-1}, in-cylinder mean and RMS velocities scaled well with flow rate. These results confirm similar findings reported for other port shapes.[12,15]

4.2. *Effects of intake jet direction, port deactivation, throttling and EGR*

Having established the accuracy of the predictions, the structure of the flow with the production ports and the similarity of air and liquid flows, the intake ports were not included in the numerical grid for the following investigations, although the cylinder head design, bore and length were identical with those in the previous simulations. The fluid medium was air in all cases. Table I provides a summary of the flow configurations investigated. The direction of the intake jets into the engine cylinder was altered in order to simulate flow through different types of inlet port. The notation of the inlet flow angles specified is shown in Figure 6. The intake flow was directed at various angles α relative to the valve axes in the y–z planes to study the effect of port centreline shape on in-cylinder motion. Similarly, air was introduced at different angles β to simulate flow inside an engine with helical-type ports and at various angles γ to model flows resulting from swirl-type ports. As these angles lie in planes which are perpendiclar to each other, it is possible to define flow entry at a particular value of, for example, angle β while maintaining angle γ equal to zero. It should be noted that although in production ports swirl- or helical-type motions are introduced by flow entry angles involving a combination of angles β and γ, in this investigation the effect of each of these angles was considered separately to allow the effects of different generic port centreline shapes to be studied in isolation. The influence of port deactivation, throttling and exhaust gas recirculation was also studied.

Table I. List of flow cases predicted without modelling inlet ports

Case no.	Port 1				Port 2				Volume-averaged K ($m^2\ s^{-2}$)	Valve seat Valve seat recirculation simulated?
	α (°)	β (°)	γ (°)	Mass flow rate (kg s^{-1})	α (°)	β (°)	γ (°)	Mass flow rate (kg s^{-1})		
1	0	0	0	0·03216	0	0	0	0·03216	24·40	No
2	30	0	0	0·03216	0	0	0	0·03216	18·69	No
3	0	0	0	0·03216	0	30	0	0·03216	25·82	No
4	0	30	0	0·03216	0	30	0	0·03216	25·25	No
5	0	0	0	0·03216	0	0	0	0·03216	28·04	Yes
6	0	0	0	0·03216	0	0	0	0	14·11	Yes
7	0	0	8	0·03216	0	0	0	0	13·52	Yes
8	0	0	30	0·03216	0	0	0	0	13·62	Yes
9	50	0	0	0·03216	0	0	0	0	12·24	Yes
10	0	0	0	0·03216	0	0	0	0·01286	15·75	Yes

The volume-averaged turbulent kinetic energy (K) was also evaluated for each of the cases modelled in order to provide an estimate of the total amount of k generated in the cylinder. K is defined as

$$K = \sum kv/V, \tag{1}$$

where k is the turbulence kinetic energy in a cell, v is the volume of the cell and V is the total volume of all cells in the grid.

Flow with both inlet valves open. Figure 7(a) presents the vectors in the $x = -17{\cdot}6$ mm plane for $\alpha = \beta = \gamma = 0°$ and $Q_T = 2Q_{P1} = 2Q_{P2} = 0{\cdot}06432$ kg s^{-1}. The mean velocity of the air at the

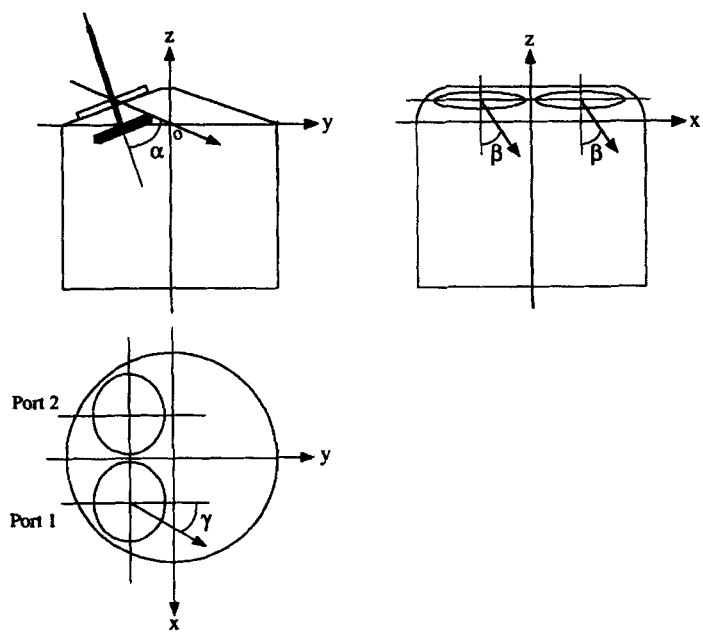

Figure 6. Inclination angles of intake flow relative to inlet valve axes

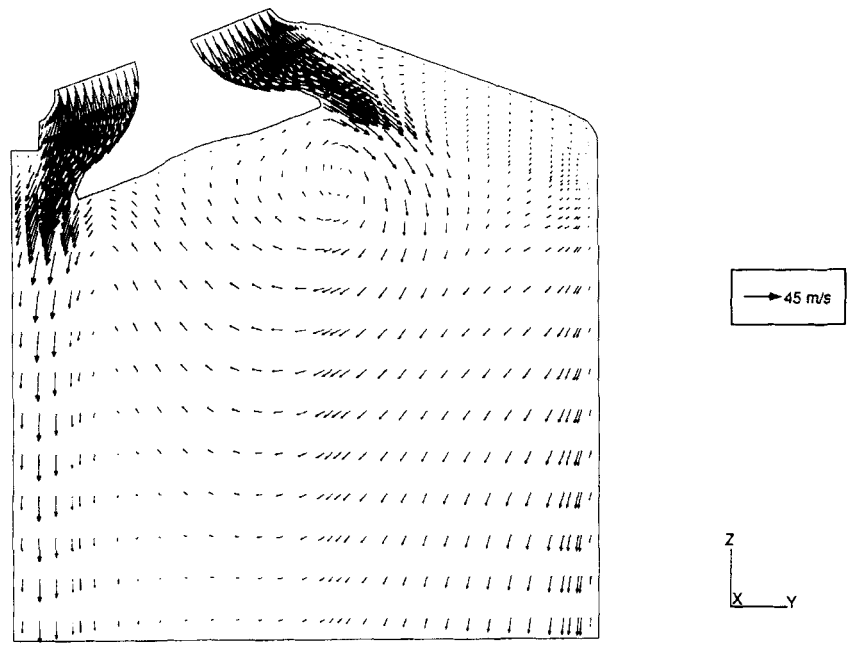

Figure 7(a). Velocity vectors in $x = -17{\cdot}6$ mm plane for $\alpha = 0°$ intake jet direction through both ports

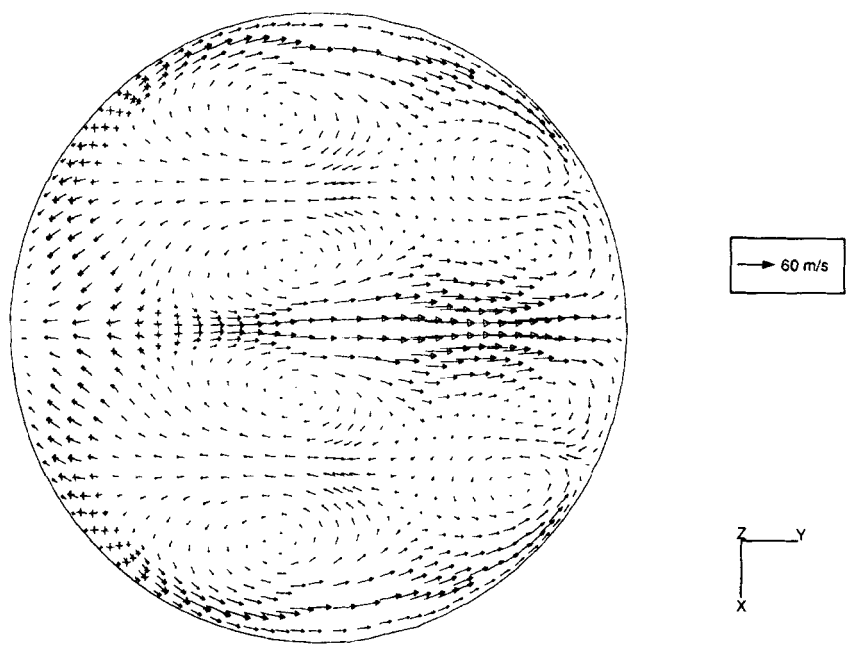

Figure 7(b). Velocity vectors in $z = -10$ mm plane for $\alpha = 0°$ intake jet direction through both ports

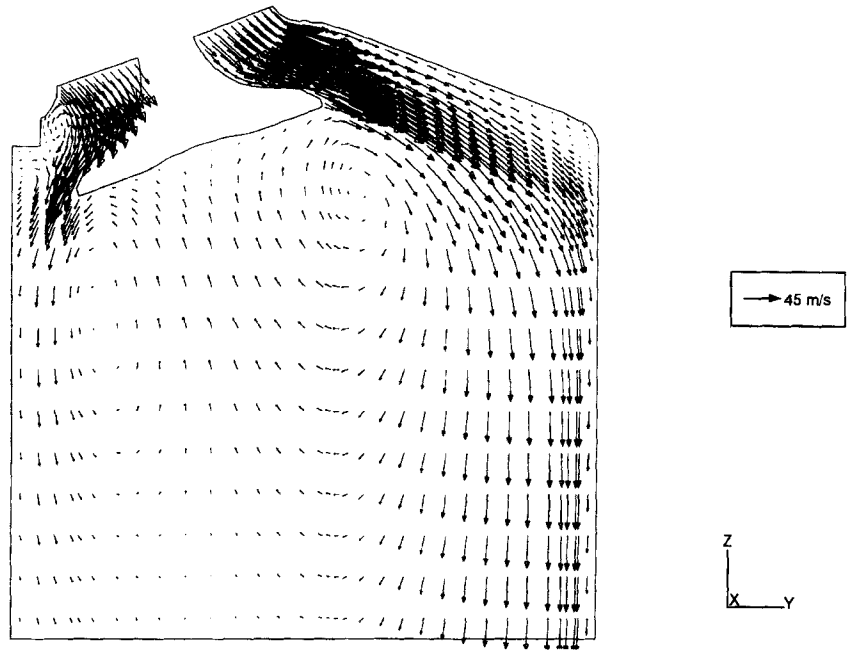

Figure 7(c). Velocity vectors in $x = -17{\cdot}6$ mm plane for $\alpha = 30°$ intake jet direction through both ports

entry plane is 45 m s^{-1}. The intake jets shown at either side of the valve head contain an identical mass of air, so that velocities inside the jet are similar on either side of the valve. The flow in the central region of the plane comprises a large tumble-like vortex in which velocities vary from 5 to 13·5 m s^{-1}. A recirculation region is present near the combustion chamber roof. Air flowing upwards in the vortex strikes the bottom of the valve head and combines with the flow along the left cylinder wall. On the right, flow is introduced into this plane from other areas by swirl.

The flow structure in the $z = -10$ mm plane for this case is presented in Figure 7(b). Several groups of swirling vortices are apparent. Strong velocities up to 50 m s^{-1} are evident close to the wall and in the jet flow directed to the right away from the centre. The numerous small vortices that are present in this flow indicate than an $\alpha = 0°$ angle for the intake jets may not be advantageous for the creation of strong organized in-cylinder air motion during induction. The volume-averaged turbulence kinetic energy for this configuration was 24·40 m^2 s^{-2}.

With α increased to 30°, $\beta = \gamma = 0°$ and $Q_T = 2Q_{P1} = 2Q_{P2}$ maintained at 0·06432 kg s^{-1}, the flow structure shows many similarities to that predicted with the inlet ports modelled (Figure 4(a)), as shown by the $x = -17{\cdot}6$ mm plane vectors in Figure 7(c): the toroidal ring vortex under the valve is similar in both figures, but the separation near the valve seat is smaller in Figure 7(c). There are four main differences from the flow produced with $\alpha = 0°$ (Figure 7(a)): when $\alpha = 30°$, the toroidal vortex is better-defined, the tumble-like motion is enhanced, the intake jet on the right of the valve extends to the roof of the chamber and a recirculation is formed on the seat along the left side of the valve. K is 18·69 m^2 s^{-2}, around 30 per cent lower than that obtained with $\alpha = 0°$.

The influence of helical-type ports on the flow was examined by introducing intake air at various angles β to the valve axes (see Figure 6), with $\alpha = \gamma = 0°$ in both ports. At first, air was introduced at $\beta = 30°$, i.e. directed away from the valve in the negative x-direction, through port 2 and $\beta = 0°$ through port 1. $Q_{P1} = Q_{P2} = 0{\cdot}03216$ kg s^{-1}, as for the two cases described above. Figure 8(a)

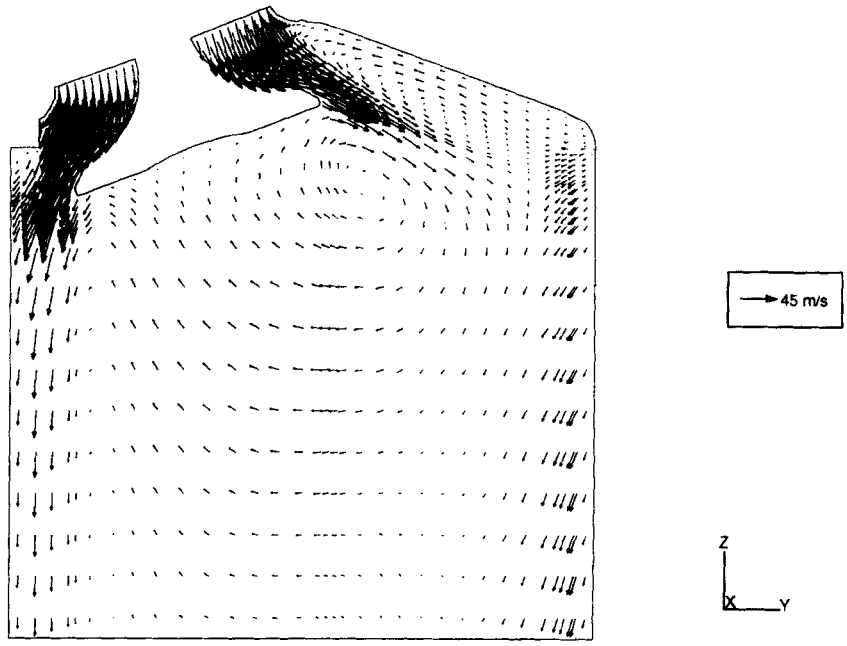

Figure 8(a). Velocity vectors in $x = -17{\cdot}6$ mm plane for $\beta = 30°$ intake jet direction through port 2

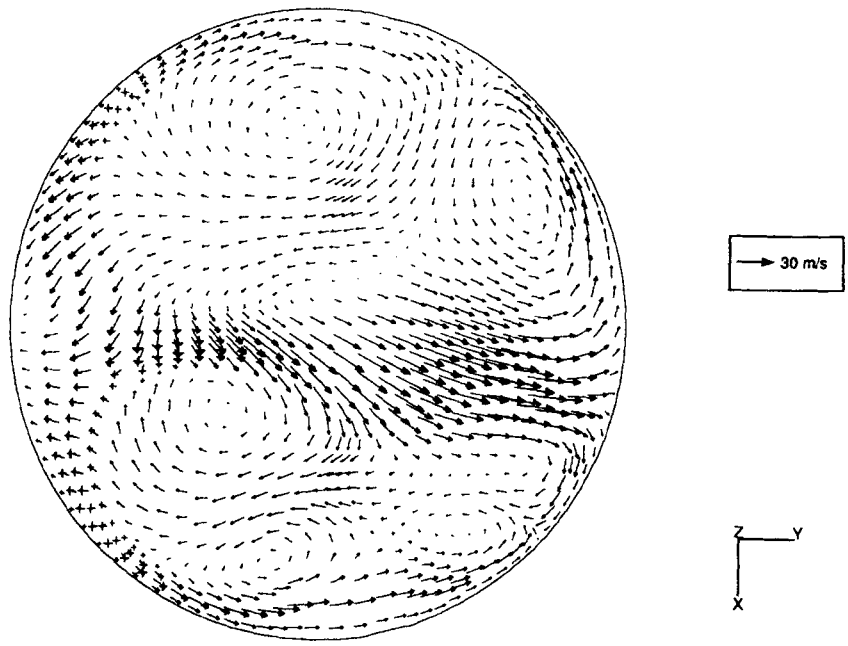

Figure 8(b). Velocity vectors in $z = -10$ mm plane for $\beta = 30°$ intake jet direction through port 2

presents velocity vectors in the vertical plane through the centre of port 2 ($x = -17{\cdot}6$ mm). The flow structure in the $x = 17{\cdot}6$ mm plane through port 1 was very similar to that shown in Figure 7(a) for the flow with $\alpha = \beta = \gamma = 0°$ and is not presented. The mean flow patterns in the $x = -17{\cdot}6$ mm and 17·6 mm planes showed small differences: velocities in the recirculation formed beneath port 2 near the chamber roof are larger but the flows are essentially similar. No valve seat separation is predicted on the left of the valve in either plane as $\alpha = 0°$.

In horizontal planes (the vectors in the $z = -10$ mm plane are shown in Figure 8(b)) the flow is asymmetric owing to the different angles of entry β through the two ports, with lower velocities underneath port 2—in the top half of the figure—than underneath port 1. The flow from port 1 has generated two groups of counter-rotating swirling vortices similar to those noted in Figure 7(b) for the case where flow was introduced into both ports at angle $\alpha = 0°$. However, these vortices have shifted in position relative to those of Figure 7(b) owing to the strong air motion introduced from port 2 combining with that from port 1 and, compared with the $\beta = 0°$ cases above, swirl is enhanced.

Steady flow air motion in an engine with two identical helical-type ports was simulated by introducing intake flow at $\beta = 30°$ through both ports and $Q_T = 2Q_{P1} = 2Q_{P2} = 0{\cdot}06432$ kg s^{-1}. In the $x = -17{\cdot}6$ mm plane through port 2, all the flow features already described for Figure 8(a) were also present and velocity magnitudes were very similar too. This is not unexpected, since the conditions for flow entry through port 2 are identical with those specified for the previous flow case. The flow field in the vertical $x = 17{\cdot}6$ mm plane through port 1, presented in Figure 9, does, however, show differences from those calculated in the plane of port 1 with $\alpha = \beta = 0°$ (cf. Figure 7(a)) as well as with $\alpha = 0°$ and $\beta = 30°$ (cf. Figure 8(a)). A stronger intake jet is found to the right of the valve in Figure 9 which occupies a larger area and extends to the roof of the chamber. The magnitude of K with both port flows directed at $\beta = 30°$ is very similar to that calculated with one port with $\beta = 0°$ and the other with $\beta = 30°$.

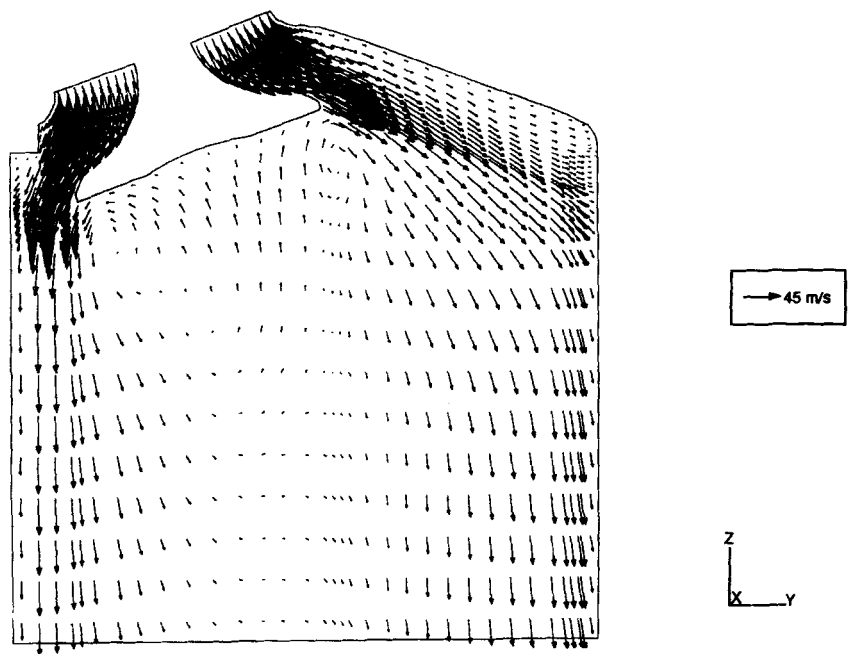

Figure 9. Velocity vectors in $x = 17{\cdot}6$ mm plane for $\beta = 30°$ intake jet direction through both ports

Visualization of the flow with laser sheet techniques revealed the presence of the separation region formed along the seat on the left of the valve at 10 mm lift, which was predicted when the port shapes were fully modelled (see e.g. Figure 4(a)). However, this separation was not modelled in any of the four cases described so far in this subsection. In order to establish whether modelling this separation would affect significantly the predicted flow structures, this region was modelled in both ports as a solid wall, using the size and shape of the region determined from the flow visualization.

Figure 10 presents the resulting flow field in a vertical plane through the centre of port 1. $Q_{P1}/2 = Q_{P2}/2 = 0{\cdot}03216$ kg s^{-1} and $\alpha = \beta = \gamma = 0°$ were specified. As a consequence of the flow restriction due to the separation, velocities at the inlet, at around 58 m s^{-1}, are higher for this configuration than when no separation was modelled. The flow to the right of Figure 10 shows little change from the case where no separation was simulated (cf. Figure 7(a)). The largest difference arising from the separation is found on the left of the valve, where the area through which air can enter the cylinder has been reduced. Otherwise, all flow features in both horizontal and vertical planes are almost identical with those already discussed for Figures 7(a) and 7(b). K, at 28·05 m^2 s^{-2}, is around 15 per cent higher than for the case where the separation was not modelled.

As it is likely that in ports of similar inclination a separation region will be formed near the valve seat,[18] all subsequent predictions were made with this separation region modelled, to provide a more realistic representation of the in-cylinder flow structure.

Effect of port deactivation. By keeping one of the two inlet valves closed, it is possible to generate more pronounced swirl and tumble motions than those produced with both valves open, leading to higher turbulence intensities near the combustion chamber on approach to TDC of compression.[2,19–21] This can give rise to more rapid combustion and give significant improvements in fuel economy. For this reason the influence of port deactivation was assessed for steady flow conditions.

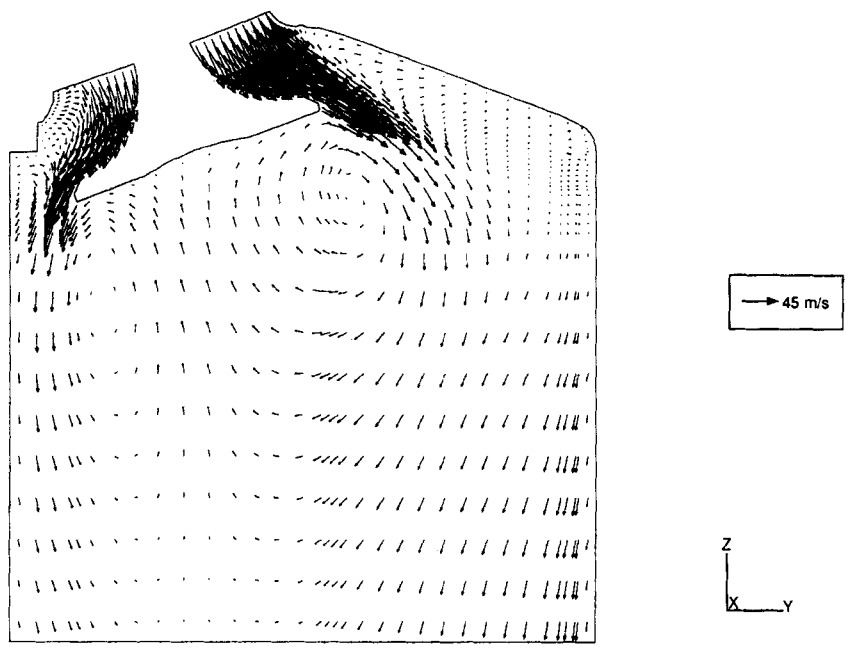

Figure 10. Velocity vectors in $x = -17{\cdot}6$ mm plane for $\alpha = \beta = 0°$ intake jet directions with simulation of valve seat recirculation

At first, no flow was specified through port 2 and air at $Q_{P1} = 0{\cdot}03216$ kg s^{-1} was introduced through port 1 with $\alpha = \beta = 0°$. The resulting flow structure in the $x = 17{\cdot}6$ mm plane through port 1 is shown in Figure 11(a). The jet to the right of the valve extends closer to the cylinder wall, the left side of the toroidal vortex under the valve is larger and as a result the tumble motion is far less pronounced in this plane than with both ports open (Figures 7(a) and 10). Velocity magnitudes in this plane are similar to those in Figures 7(a) and 10, but were significantly lower under port 2 (results not shown for economy of presentation), as expected owing to the reduced total flow rate into the cylinder. The flow in the $z = -10$ mm plane (Figure 11(b)) is asymmetric, as might be expected. In general an anticlockwise swirl motion can be identified along the cylinder wall, but a number of vortices are present and no clear swirl pattern is formed. K for this case, $14{\cdot}12$ m^2 s^{-2}, is almost 50 per cent of that with both inlet valves open, as there is no interaction between the jets issuing from the two ports and velocity gradients are less steep.

The above results showed that a well-defined swirl structure is not produced at $z = -10$ mm and turbulence levels are decreased when one port is deactivated. Therefore, in an attempt to accentuate swirl in the engine cylinder with port 2 closed, two further cases were modelled, with $Q_{P1} = 0{\cdot}03216$ kg s^{-1} and directed at $\gamma = 8°$ and 30° and $\alpha = \beta = 0°$. The 8° angle represents the limit of possible modification for the current Zetec cylinder head design, while the 30° angle was selected as an extreme case which might achieve more intense swirl but would necessitate considerable design modifications. With $\gamma = 8°$ the flow structures in horizontal and vertical planes were qualitatively and quantitatively very similar to those shown in Figure 11 with $\gamma = 0°$. When γ was altered to 30°, no significant change was again apparent in the flow structure compared with the $\gamma = 0°$ results. Hence it would appear that altering the intake air direction angle γ while one inlet valve is kept closed has relatively little influence on the flow characteristics.

The results of Figure 11(a) showed that with port deactivation and flow introduced into the cylinder in a direction parallel to the valve axis, i.e. at $\alpha = 0°$, much of the air is directed in a jet passing to the

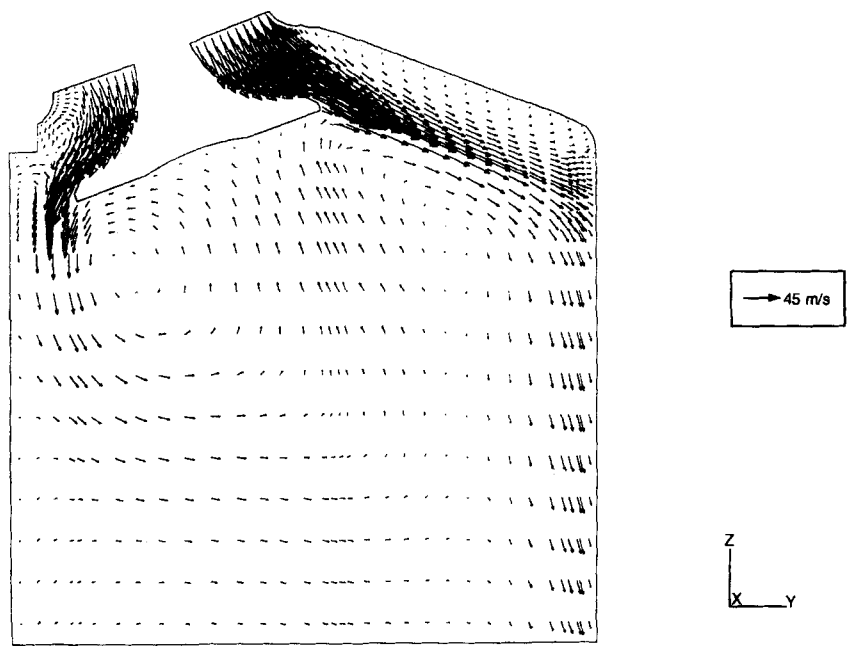

Figure 11(a). Velocity vectors in $x = 17{\cdot}6$ mm plane with port 2 closed

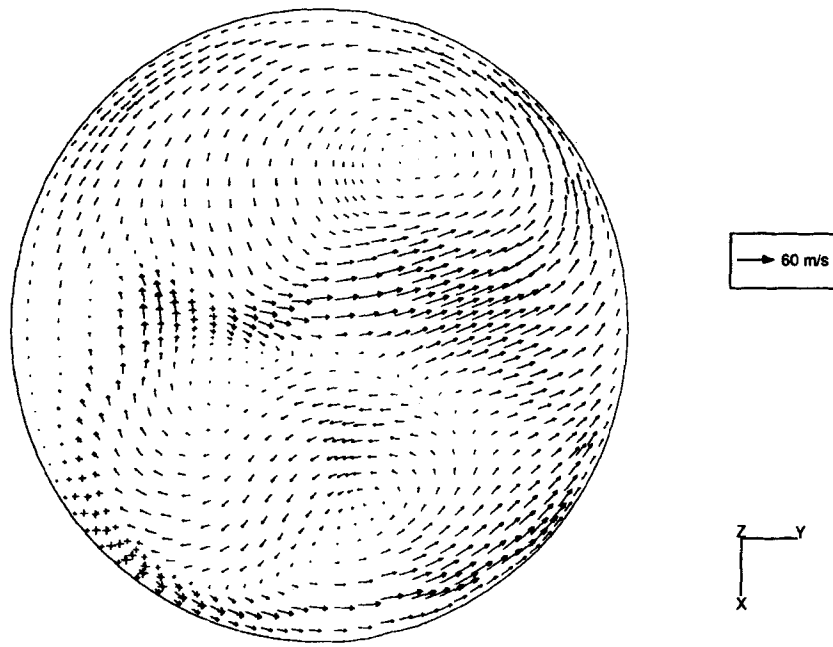

Figure 11(b). Velocity vectors in $z = -10$ mm plane with port 2 closed

left of the inlet valve. Investigations were therefore made to determine whether air directed at $\alpha = 50°$ and $\beta = \gamma = 0°$ through port 1 would improve the flow characteristics. Again Q_{P1} is 0·03216 kg s^{-1}. The vectors in the plane $x = 17{\cdot}6$ mm are shown in Figure 12(a). Intense air motion is produced to the right of the valve and down the cylinder wall. Velocities up to 100 and 70 m s^{-1} have been computed in the valve gap and adjacent to the cylinder wall on the right respectively. A large recirculation has been created to the left of the valve which inhibits air from entering the cylinder through this region. As a result a single vortex with low-magnitude velocities everywhere except near the right-hand wall is formed over most of the cylinder.

Figure 12(b) indicates that a better-defined swirl motion is produced in the cylinder with this configuration compared with Figure 11(b). An anticlockwise swirling motion with magnitude around 45 m s^{-1} is formed along the wall. Almost all the air in this plane is moving in the direction of the swirling flow.

This configuration provides the most intense in-cylinder flow motion, which enhances swirl levels and the in-cylinder jet flow. This shows promise for the generation of high tumble ratio under motored conditions, as the strong jet along the cylinder wall will interact with and be redirected by the piston and could thus form a very intense tumble motion. However, the K-value calculated for this combination is the lowest of all cases predited.

Effect of port throttling and exhaust gas recirculation. In the previous subsection the effect of port deactivation on the flow was assessed. However, in many engines, port throttling rather than deactivation is used, often combined with EGR introduced through the throttled port. This strategy has been found to be promising for charge stratification in the cylinders of multivalve engines.[10,22,23] To simulate port throttling and EGR distribution in the engine cylinder, predictions were made with the lift set at 10 mm and $\alpha = \beta = \gamma = 0°$ for both ports. Air at 0·03216 kg s^{-1} was introduced

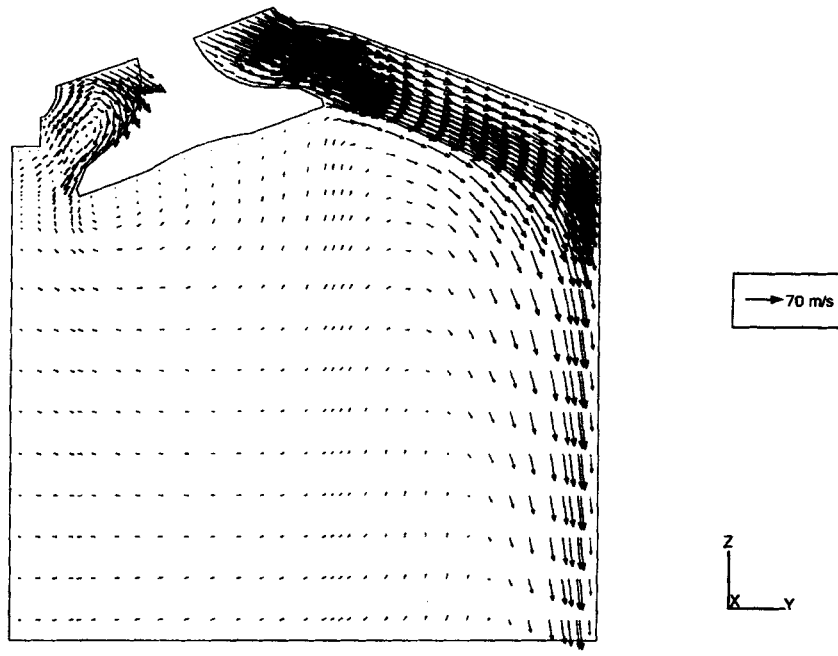

Figure 12(a). Velocity vectors in $x = 17{\cdot}6$ mm plane with port 2 closed and $\alpha = 50°$ intake jet direction through port 1

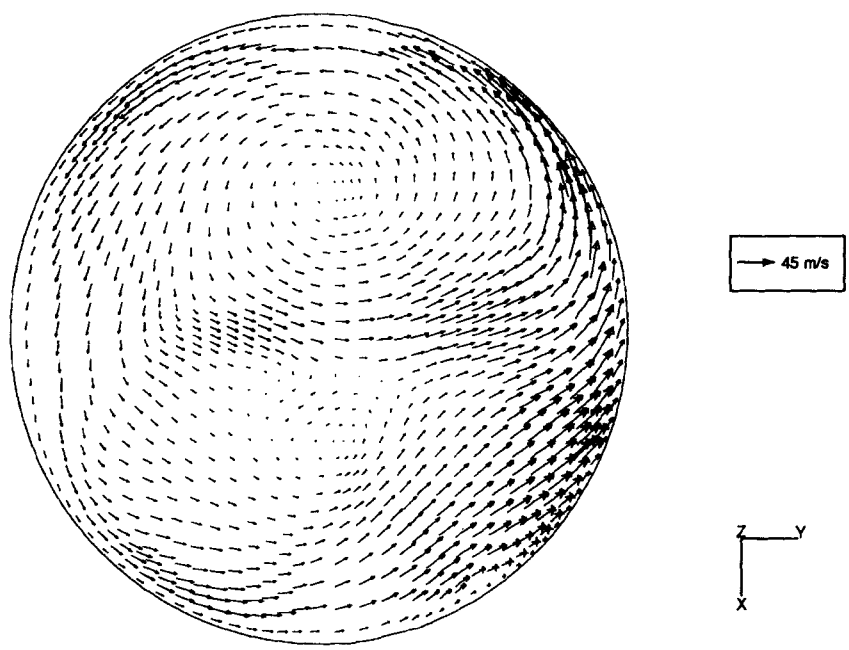

Figure 12(b). Velocity vectors in $z = -10$ mm plane with port 2 closed and $\alpha = 50°$ intake jet direction through port 1

through port 1, while simulated exhaust gas at 0·01286 kg s^{-1} (40 per cent of the flow rate through port 1) was admitted through port 2. The EGR fluid had identical properties to that of the air but was marked as a passive scalar in order to determine the distribution of air and EGR fluid in the cylinder.

The predicted flow field in the $z = -10$ mm plane is shown in Figure 13(a). The flow structure is asymmetric owing to the different flow rates through the ports; gas velocities are lower at the top than at the bottom for the same reason. A number of counter-rotating vortices are formed and the swirl, although predominantly anticlockwise, is not unidirectional. The swirl structure shows similarities to that shown in Figure 11(b), for which port 1 was deactivated.

The concentration of EGR fluid in the same plane is shown in Figure 13(b). The highest concentrations of exhaust gas, 82 per cent–96 per cent, are located in the upper portion of Figure 13(b), i.e. below port 1. The stronger air flow from port 1 maintains EGR levels in the region underneath port 2 at around 4 per cent–25 per cent. Therefore this configuration appears promising for charge stratification.

The results indicate that modifications to the shape and orientation of the inlet ports could allow a combination of tumble and swirl to be generated. This could enhance pre-ignition turbulence,[5] especially as a direct correlation between the intensity of the intake-generated flow and combustion delay and duration has been established.[7] Of course, dynamic effects are present in a reciprocating engine and interpretation of the above results must be made with care. However, the present predictions confirm the finding of Stone *et al.*,[21] obtained through steady air flow rig tests, that valve disablement in a dual-intake pent-roof chamber leads to an increase in tumble and swirl. It should be noted as well that both the experiments and predictions of Henriot *et al.*[19] also revealed a pronounced swirl and tumble in a motored engine with only one intake valve operating. Therefore the present results indicate that steady flow CFD predictions of the in-cylinder flows can provide useful indications of the effect of port shape, throttling and deactivation at a significantly reduced

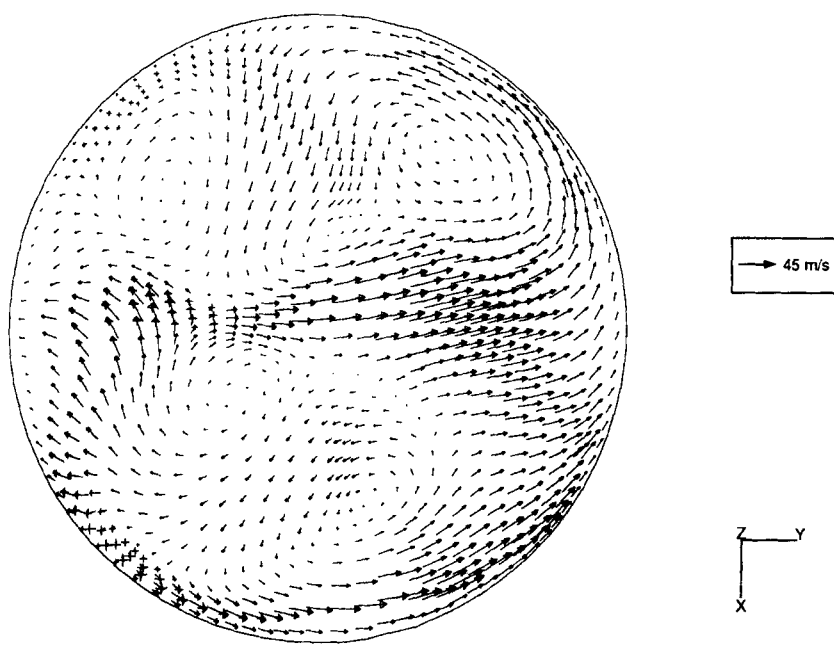

Figure 13(a). Velocity vectors in $z = -10$ mm plane with exhaust gas introduced through port 2

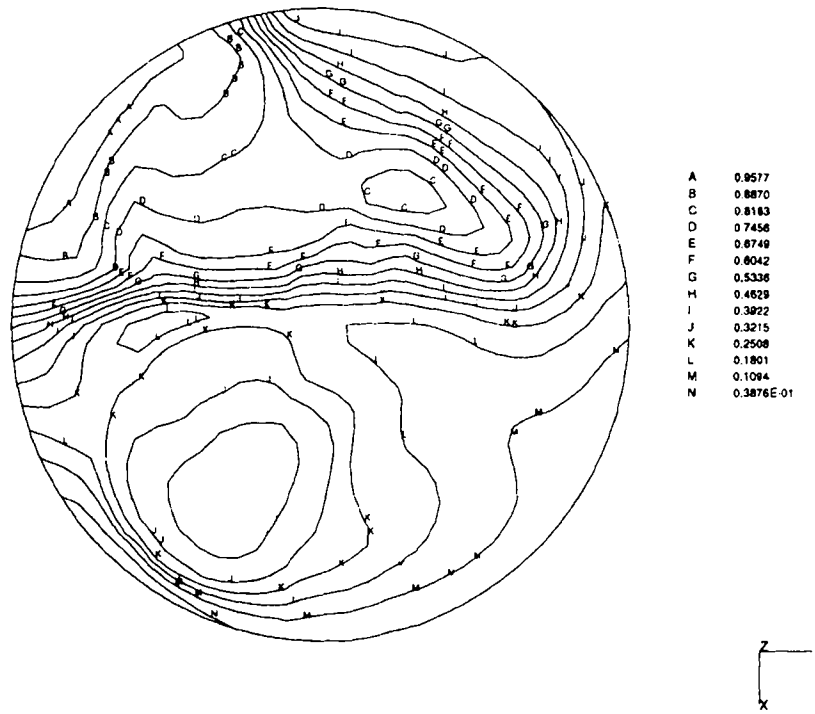

Figure 13(b). Contours of exhaust gas concentration in $z = -10$ mm plane with exhaust gas introduced through port 2. Contour values indicate fraction of EGR

computational cost before more extensive calculations are made under motored and/or firing conditions.

5. CONCLUSIONS

A study of fluid motion inside thermal internal combustion engine cylinders was reported. The flow inside the ports and cylinder of a Ford Zetec engine at 5 and 10 mm inlet valve lifts was modelled using CFD and investigated experimentally by flow visualization and LDA. Comparisons of axial and transverse velocity components showed that all features of the flows were successfully predicted and very good agreement between the CFD and LDA results was achieved at most locations within the ports and cylinder. Mean and RMS velocities scaled well with flow rate and simulations of air and liquid flows at the same *Re* predicted similar flow patterns.

The influence of intake flow direction on the in-cylinder velocity and turbulence characteristics was investigated by varying the angles of entry of the intake jets α, β and γ in the y–z, x–z and x–y planes relative to the valve axes respectively. With both ports fully open, an increase in α from 0° to 30° results in an enhancement of tumble. An increase in β from 0° to 30° produces a slight enhancement of in-cylinder swirl. Variation of the intake angle γ combined with port deactivation was found to have no significant effect. In contrast, port deactivation with $\alpha = 50°$ gave rise to the most intense in-cylinder flow motion, which enhanced swirl levels and shows promise for generation of strong tumble under motored conditions.

Stratification of exhaust gas and air was simulated in the engine cylinder under steady flow conditions by admitting air through a wide-open port and EGR through a throttled port. Concentrations of exhaust gas of 80 per cent–95 per cent were achieved below the EGR port, while EGR levels in the other half of the cylinder were on average about 10 per cent.

The highest values of the volume-averaged turbulence kinetic energy were obtained with $\alpha = \gamma = 0°$ and $\beta = 0°$ or 30°; these values decreased by around 50 per cent with port throttling or deactivation or when α was increased to 30°.

The results have shown that steady flow CFD predictions of good accuracy can be made which may be used to obtain an initial assessment of port characteristics and thus allow engine flow control strategies to be scrutinized before more complex and time-consuming motored and firing engine predictions are undertaken.

ACKNOWLEDGEMENTS

The authors acknowledge support from the EPSRC under grant GR/J65693 and from Ford Motor Company Limited for the work presented in this paper.

APPENDIX: NOMENCLATURE

d	hydraulic diameter of port inlet plane, $d = 37$ mm
k	kinetic energy of turbulence ($m^2\ s^{-2}$)
K	volume-averaged kinetic energy of turbulence ($m^2\ s^{-2}$)
Q_{P1}, Q_{P2}	mass flow rates through ports 1 and 2 respectively (kg s^{-1})
Q_T	total mass flow rate through both ports (kg s^{-1})
Re	flow Reynolds number, $Re = U_T d/v$
u'	RMS velocity component in x-direction (m s^{-1})
U	mean velocity component in x-direction (m s^{-1})
U_T	bulk flow velocity at port inlet plane (m s^{-1})
v	volume of one cell in grid (m^3)
v'	RMS velocity component in y-direction (m s^{-1})
V	mean velocity component in y-direction (m s^{-1}); total volume of all cells in grid (m^3)
w'	RMS velocity component in z-direction (m s^{-1})
W	mean velocity component in z-direction (m s^{-1})

Greek letters

α	angle of intake flow in y–z plane (deg)
β	angle of intake flow in x–z plane (deg)
γ	angle of intake flow in x–y plane (deg)
ν	kinematic viscosity of fluid ($m^2\ s^{-1}$)

REFERENCES

1. A. D. Gosman, Y. Y. Tsui and C. Vafidis, 'Flow in a model engine with a shrouded valve—a combined experimental and computational study', *SAE Paper 850498*, 1985.
2. B. Khalighi, 'Intake generated swirl and tumble motions in a 4-valve engine with various intake configurations—flow visualization and particle tracking velocimetry', *SAE Paper 900059*, 1990.
3. M. Rönnbäck, W. X. Le and J.-R. Linna, 'Study of induction tumble by particle tracking velocimetry in a 4-valve engine', *SAE Paper 912376*, 1991.

4. S. Furuno, S. Iguchi, K. Oishi and T. Inoue, 'The effects of "inclination angle of swirl axis" on turbulence characteristics in a 4-valve lean burn engine with SCV', *SAE Paper 902139*, 1990.
5. C. Arcoumanis, Z. Hu and J. H. Whitelaw, 'Steady-flow characterization of tumble-generating four-valve cylinder heads', *Proc. I.Mech.E., J. Automobile Eng.*, **207**, 203–210 (1993).
6. C. D. de Boer, R. J. R. Johns, D. W. Grigg, B. M. Train, I. Denbratt and J.-R. Linna, 'Refinement with performance and economy for four-valve automotive engines', *Proc. I.Mech.E. Conf. on Automotive Power Systems—Environment and Conservation*, Institution of Mechanical Engineers, London, 1990, Paper C394/053, pp. 147–155.
7. H. Endres, H.-J. Neusser and R. Wurms, 'Influence of swirl and tumble on economy and emissions of multivalve engines', *SAE Paper 920576*, 1992.
8. Y. Kiyota, K. Akishino and H. Ando, 'Concept of lean combustion by barrel-stratification', *SAE Paper 920678*, 1992.
9. J. Stokes, T. H. Lake, M. J. Christie and I. Denbratt, 'Improving the NO_x/fuel economy trade-off for gasoline engines with the CCVS combustion system', *SAE Paper 940482*, 1994.
10. I.-Y. Ohm, H.-S. Ahn, W.-J. Lee, W.-T. Kim, S.-S. Park and D.-U. Lee, 'Development of HMC axially stratified lean combustion engine', *SAE Paper 930879*, 1993.
11. G. Morris and P. Lake, 'The Ford Zeta engine family: Paper 3—Engine development', *Proc. I.Mech.E. Conf. Autotech '91*, Institution of Mechanical Engineers, London, 1991, Paper C427/243, pp. 1–10.
12. R. S. W. Cheung, S. Nadarajah, M. J. Tindal and M. Yianneskis, 'An experimental study of velocity and Reynolds stress distributions in a production engine inlet port under steady flow conditions', *SAE Paper 900058*, 1990.
13. Z. Mahmood and M. Yianneskis, 'Velocity and turbulence characteristics of steady flow processes in the ports and cylinder of a Ford Zetec engine', *Internal Rep. EM/95/02*, Mechanical Engineering Department, King's College London, 1995.
14. *STAR-CD Version 2.21 User Manual*, Computational Dynamics Ltd., London, 1994.
15. A. Chen, K. C. Lee, M. Yianneskis and G. Ganti, 'Velocity characteristics of steady flow through a straight generic inlet port', *Int. j. numer. methods fluids*, **21**, 571–590 (1995).
16. R. I. Issa, 'Solution of the implicitly discretized fluid flow equations by operator-splitting', *J. Comput. Phys.*, **62**, 40– 65 (1985).
17. S. Balabani and M. Yianneskis, 'An experimental study of mean flow and turbulence structure of the cross-flow over tube bundles', *Proc. I.Mech.E., J. Mech. Eng. Sci.*, **210**, 317–331 (1996).
18. K. C. Lee, K. O. Suen, M. Yianneskis and G. Ganti, 'Steady flow characteristics of two generic inlet ports', *Proc. Sixth Int. Symp. on Applications of Laser Techniques to Fluid Mechanics*, Ladoan, Lisbon, July 1992, pp. 29.4.1–29.4.7.
19. S. Henriot, J. F. Le Coz and P. Pinchon, 'Three-dimensional modelling of flow and turbulence in a four-valve spark-ignition engine—comparisons with LDV measurements', *SAE Paper 890843*, 1989.
20. J. C. Kent, A. Mikulec, A. A. Adamczyk, S. R. Mueller, R. A. Stein and C. C. Warren, 'Observations on the effects of intake-generated swirl and tumble on combustion duration', *SAE Paper 892096*, 1989.
21. C. R. Stone, T. R. Carden and I. Podmore, 'Analysis of the effect of inlet valve disablement on swirl, combustion and emissions in a spark-ignition engine', *Proc. I.Mech.E., J. Automobile Eng.*, **207**, 295–305 (1993).
22. T. G. Baker, C. J. E. Nightingale and D. J. Myers, 'Port throttles applied to a high performance S.I. engine', *Proc. I.Mech.E. Conf. on Combustion in Engines*, Institution of Mechanical Engineers, London, 1992, Paper C448/032, pp. 165–174.
23. H. Endres, H. Schulte and R. Krebs, 'Combustion system development trends for multi-valve gasoline engines', *SAE Paper 900652*, 1990.